

Critical phenomena in colloid–polymer mixtures: interfacial tension, order parameter, susceptibility and coexistence diameter

R. L. C. Vink, J. Horbach, and K. Binder

Institut für Physik, Johannes Gutenberg-Universität, D-55099 Mainz, Staudinger Weg 7, Germany

(Dated: September 4, 2018)

The critical behavior of a model colloid–polymer mixture, the so-called AO model, is studied using computer simulations and finite size scaling techniques. Investigated are the interfacial tension, the order parameter, the susceptibility and the coexistence diameter. Our results clearly show that the interfacial tension vanishes at the critical point with exponent $2\nu \approx 1.26$. This is in good agreement with the 3D Ising exponent. Also calculated are critical amplitude ratios, which are shown to be compatible with the corresponding 3D Ising values. We additionally identify a number of subtleties that are encountered when finite size scaling is applied to the AO model. In particular, we find that the finite size extrapolation of the interfacial tension is most consistent when logarithmic size dependences are ignored. This finding is in agreement with the work of Berg *et al.* [Phys. Rev. B, **47**, 497 (1993)].

PACS numbers: 61.20.Ja, 64.75.+g

I. INTRODUCTION

By adding non-adsorbing polymer to a colloidal suspension, phase separation may be induced. This leads to the formation of two coexisting fluid phases, separated by an interface [1, 2]. The phases are characterized by their colloid density, which is high in one phase, and low in the other. In order to make the analogy to the fluid–vapor transition in atomic liquids, the colloid rich phase is usually called the colloidal liquid, and the colloid poor phase the colloidal vapor. Obviously, the density of the polymers is exactly the opposite: high in the colloidal vapor and low in the colloidal liquid.

In the vicinity of the critical point, a number of important physical quantities are described by simple power laws of the form At^B . Here, t is some measure of distance from the critical point, A is called the critical amplitude, and B the critical exponent [3]. To describe the critical phase behavior, one thus needs to determine the location of the critical point, the critical exponents and the critical amplitudes. These quantities can for instance be obtained in computer simulations, provided finite size scaling methods are used. Finite size scaling is required because the correlation length diverges at the critical point. Since the accessible system size in a simulation is finite, the true critical behavior is obscured as soon as the correlation length exceeds the size of the simulation box [3, 4]. Finite size scaling offers a way to properly extrapolate the data obtained in simulations to the thermodynamic (=infinite system) limit [5].

In this work, we study the critical behavior of the colloid–polymer model introduced by Asakura and Oosawa [6, 7] (the so-called AO model). In previous simulations, we have determined the critical point of the AO model (for one choice of colloid–to–polymer size ratio) and we have provided evidence that this system belongs to the 3D Ising universality class [8, 9]. However, we have not yet studied in detail whether we can recover the critical exponents, nor have we determined the crit-

ical amplitudes. The latter quantities are of interest because certain critical amplitude ratios are predicted to be universal. In this work we combine computer simulations and finite size scaling to address these issues. The quantities that we consider are the order parameter, susceptibility, coexistence diameter, and interfacial tension, whereby the critical point is approached along different paths: from the one–phase region, the two–phase region, and along the coexistence line.

The AO interfacial tension is of particular importance, because it gives an indication of the strength of capillary waves. This is an issue in (mean–field) density functional theories of the AO model. Following Ref. 10, the strength of the capillary waves is estimated by $\omega = k_B T / (4\pi\sigma\xi^2)$, with σ the interfacial tension, ξ the correlation length in the two–phase region, T the temperature, and k_B the Boltzmann constant. For 3D Ising critical behavior, hyperscaling implies that ω is constant in the critical regime. Note that this constant is universal and given by $\omega \approx 0.8$ [11]. In contrast, for mean–field critical behavior, one would observe a decay of the form $\omega \propto t^{-1/2}$. The mean–field behavior and the 3D Ising behavior of the capillary strength are thus profoundly different. Therefore, it is important to establish the universality class of the AO model. For this purpose, an analysis of the interfacial tension is particularly suitable. To determine the critical behavior of the interfacial tension, finite size scaling methods can be used that do not require prior knowledge of the universality class. This enables a direct measurement of the critical exponent, and the corresponding critical amplitude. For the AO model, we obtain for the interfacial tension a critical exponent $2\nu = 1.26$, which is in excellent agreement with the 3D Ising value.

The critical amplitudes are used to test the universality of a number of critical amplitude ratios. Following Stauffer [12, 13], universality implies that only two amplitudes are required to determine the remaining amplitudes. This allows us to relate the critical amplitudes of the AO model obtained in this work, to independent

estimates obtained in experimental, theoretical, and simulation studies of completely different systems [11, 13]. We observe reasonable agreement, but emphasize that the error bars, in both our estimates and those in the literature, are quite substantial.

Note that an investigation of the AO critical behavior is far more complex than an equivalent study of the 3D Ising lattice model would be. For instance, the binodal of the AO model is asymmetric, and this gives rise to an additional critical power law for the coexistence diameter. Moreover, the AO model belongs to the class of *asymmetric binary mixtures*, which are generally difficult to simulate. In case of the AO model, the accuracy required to apply finite size scaling became available only after the recent introduction of a grand canonical Monte Carlo cluster move [9] and successive umbrella sampling [14]. Note also that the application of finite size scaling to asymmetric mixtures [15] is far less common compared to that of symmetric mixtures [4].

The outline of this paper is as follows. First, the AO model is introduced. We then move on to describe the simulation techniques used by us. Next, we explain how the order parameter, susceptibility, interfacial tension and coexistence diameter are extracted from the simulation data. The extrapolation of these quantities to the infinite system is discussed in section VI. We then present our results and end with a summary in the last section.

II. THE AO MODEL

The AO model was proposed in 1954 [6] and later independently by Vrij [7] as a simple description for colloid-polymer mixtures. In this model, colloids and polymers are treated as spheres with respective radii R_c and R_p . Hard sphere interactions are assumed between colloid-colloid (cc) and colloid-polymer (cp) pairs, while polymer-polymer (pp) pairs can interpenetrate freely. This yields the following pair potentials:

$$\begin{aligned} u_{cc}(r) &= \begin{cases} \infty & \text{for } r < 2R_c \\ 0 & \text{otherwise,} \end{cases} \\ u_{cp}(r) &= \begin{cases} \infty & \text{for } r < R_c + R_p \\ 0 & \text{otherwise,} \end{cases} \\ u_{pp}(r) &= 0, \end{aligned} \quad (1)$$

with r the distance between two particles.

Since all allowed AO configurations have zero potential energy, temperature plays a trivial role, and the phase behavior is set by the colloid to polymer size ratio $q \equiv R_p/R_c$ and the fugacities $\{z_c, z_p\}$ of colloids and polymers, respectively. The fugacity z_α is related to the chemical potential μ_α via $z_\alpha = \exp(\beta\mu_\alpha)$, with $\alpha \in \{c, p\}$.

In this work we consider a size ratio $q = 0.8$ and put $R_c \equiv 1$ to set the length scale. The colloid packing fraction is defined by $\eta_c \equiv (4\pi/3)R_c^3 N_c/V$, and the polymer

packing fraction by $\eta_p \equiv (4\pi/3)R_p^3 N_p/V$. Here, N_c (N_p) denotes the number of colloids (polymers) inside the simulation cell and V the volume of the simulation cell. Following convention, we use the quantity $\eta_p^r \equiv z_p(4\pi/3)R_p^3$ to express the polymer fugacity, rather than z_p itself. In the literature, η_p^r is known as the polymer reservoir packing fraction. It should, however, not be confused with the actual polymer packing fraction in the system η_p .

The AO model phase separates into a colloidal vapor and colloidal liquid, provided q and η_p^r are high enough [16, 17, 18, 19, 20]. For $q = 0.8$, the critical point was located at [8, 9]:

$$\begin{aligned} \eta_{p,\text{cr}}^r &= 0.766 \pm 0.002, & \eta_{p,\text{cr}} &= 0.3562 \pm 0.0006, \\ \eta_{c,\text{cr}} &= 0.1340 \pm 0.0006, & \mu_{c,\text{cr}} &= 3.063 \pm 0.003, \end{aligned} \quad (2)$$

with $\mu_{c,\text{cr}}$ the critical value of the coexistence chemical potential of the colloids and $\eta_{\alpha,\text{cr}}$ the critical value of η_α , with $\alpha \in \{p, c\}$. The above estimates were obtained using the cumulant intersection method [21], and by considering field mixing effects [22, 23].

III. SIMULATION METHOD

We simulate the AO model in the grand canonical ensemble. In this ensemble, the fugacities $\{z_c, z_p\}$ and the volume V are fixed, while the number of particles inside V fluctuates. The simulations are performed in cubic boxes with edge length L and using periodic boundary conditions. To simulate the AO model efficiently, we use a recently developed cluster move [9, 24].

A. Phase coexistence

During the simulation, we measure the probability $P(\eta_c)$ of observing a certain colloid packing fraction η_c . At phase coexistence, the distribution $P(\eta_c)$ becomes bimodal, with two peaks of equal area for the colloidal vapor and liquid phase. A natural cut-off to separate the vapor from the liquid phase is provided by the average colloid packing fraction:

$$\langle \eta_c \rangle = \int_0^\infty \eta_c P(\eta_c) d\eta_c, \quad (3)$$

where we assume $P(\eta_c)$ has been normalized to unity:

$$\int_0^\infty P(\eta_c) d\eta_c = 1. \quad (4)$$

The equal area rule simply implies that:

$$\int_0^{\langle \eta_c \rangle} P(\eta_c) d\eta_c = \int_{\langle \eta_c \rangle}^\infty P(\eta_c) d\eta_c. \quad (5)$$

The above equation provides an accurate numerical measure to determine phase coexistence [15].

B. Successive umbrella sampling

Close to the critical point, the simulation moves back and forth easily between the vapor and liquid phases. Away from the critical point, at higher polymer fugacity, the free energy barrier between the two phases increases. In that case, transitions from one phase to the other phase become more and more unlikely, and the simulation will spend most time in only one of the two phases. A crucial ingredient in our simulation is therefore the use of a biased sampling technique called successive umbrella sampling. This technique was recently developed by Virnau and Müller [14] and its purpose is to enable sampling in regions where $P(\eta_c)$, due to the free energy barrier separating the phases, is very low.

C. Histogram reweighting

A final ingredient in our simulation is the use of histogram reweighting [25]. It is based on the observation that the probability $P(\eta_c)$ measured at one set of model parameters (in this case z_c and z_p) can be used to estimate $P(\eta_c)$ at different values of these parameters. Obviously, the gain in computational efficiency is enormous because in the ideal case $P(\eta_c)$ need only be measured once.

In this work, histogram reweighting is used to locate the coexistence fugacity of the colloids. Phase coexistence is only obtained if the colloid fugacity is chosen just right. This value is in general not known at the start of the simulation. However, once $P(\eta_c|z_c, z_p)$ has been measured at colloid fugacity z_c and polymer fugacity z_p , histogram reweighting can be used to obtain $P(\eta_c|z'_c, z_p)$ at any other colloid fugacity z'_c by using the equation [5]:

$$\ln P(N_c|z'_c, z_p) = \ln P(N_c|z_c, z_p) + \left(\ln \frac{z'_c}{z_c} \right) N_c. \quad (6)$$

Note that in the above equation η_c has been replaced by the number of colloids N_c . In the simulations, we thus set the colloid fugacity to unity and apply successive umbrella sampling to obtain the corresponding probability distribution. We then use Eq.(6) to extrapolate $P(\eta_c)$ to that colloid fugacity at which the equal area rule of Eq.(5) is obeyed. In practice, it is straightforward to write an automated numerical procedure to achieve this. We emphasize here that extrapolations in z_c are exact, in the sense that no statistical or systematic errors are introduced (the term ‘‘extrapolation’’ might suggest otherwise).

Within successive umbrella sampling, states (or windows) are sampled one after the other. In the first window, the number of colloids N_c is allowed to fluctuate between 0 and 1, in the second window, N_c is allowed to fluctuate between 1 and 2, and so on. No restriction is put on the number of polymers though, so in each window N_p will fluctuate freely around some average equilibrium

value (the distribution in N_p is to a good approximation Poisson like). The crucial point is that by using successive umbrella sampling, data over the entire range from $N_c = 0$ up to some maximum is obtained (the maximum should be chosen well beyond the liquid peak). Therefore, extrapolations in z_c (which essentially ‘‘emphasize’’ the data of some windows with respect to others) can be performed without loss of accuracy.

Histogram reweighting is also used to extrapolate $P(\eta_c|z_c, z_p)$ to different polymer fugacities z'_p to obtain estimates of $P(\eta_c|z_c, z'_p)$. To this end, also the distribution of the number of polymers must be recorded for each window. Since our implementation of successive umbrella sampling only puts a bias on the number of colloids, and not on the polymers, this extrapolation will introduce an error. The accuracy of the estimated distribution deteriorates when the range $z'_p - z_p$ over which one extrapolates becomes larger. Fortunately, since we are primarily interested in the behavior close to the critical point, the range need not be large and the error introduced by histogram reweighting is small [4]. More importantly, the error can easily be checked for as will be shown later.

Note that in terms of histogram reweighting, the AO model is extremely convenient. Since the histograms that need to be maintained involve integer data only (namely numbers of particles) the problem of choosing a bin size for example does not occur.

IV. EXTRACTING OBSERVABLES

The coexistence distribution $P(\eta_c)$ is a powerful quantity because a number of important physical observables can be extracted from it. For instance, the average packing fraction of the colloidal vapor can be written as:

$$\eta_c^v = 2 \int_0^{\langle \eta_c \rangle} \eta_c P(\eta_c) d\eta_c, \quad (7)$$

and a similar expression holds for the average packing fraction of the colloidal liquid:

$$\eta_c^l = 2 \int_{\langle \eta_c \rangle}^{\infty} \eta_c P(\eta_c) d\eta_c, \quad (8)$$

with $\langle \eta_c \rangle$ given by Eq.(3). In these and following equations, the normalization condition of Eq.(4) is assumed (this also explains the origin of the factors of two in the above two equations).

For the AO model, we define in the two-phase region half the difference in colloid packing fraction between the vapor and liquid phase as order parameter. The order parameter is denoted M_c :

$$M_c \equiv \frac{\eta_c^l - \eta_c^v}{2} = \int_0^{\infty} |\eta_c - \langle \eta_c \rangle| P(\eta_c) d\eta_c, \quad (9)$$

and the coexistence diameter (or rectilinear diameter) is given by:

$$D_c \equiv \frac{\eta_c^l + \eta_c^v}{2}, \quad (10)$$

where the subscripts “c” emphasize that the definitions are expressed in terms of the colloid packing fraction, and not the polymer packing fraction.

In a similar way, we identify the “concentration susceptibility” or compressibility as the variance of the peaks in $P(\eta_c)$ [26]. In the two-phase region ($\eta_p^r > \eta_{p,cr}^r$), we define the susceptibility of the colloidal vapor as:

$$\chi_c^v = V \left[\left(2 \int_0^{\langle \eta_c \rangle} \eta_c^2 P(\eta_c) d\eta_c \right) - (\eta_c^v)^2 \right], \quad (11)$$

and the susceptibility of the colloidal liquid as:

$$\chi_c^l = V \left[\left(2 \int_{\langle \eta_c \rangle}^{\infty} \eta_c^2 P(\eta_c) d\eta_c \right) - (\eta_c^l)^2 \right], \quad (12)$$

where the factors of two are again consequence of the normalization condition of Eq.(4). Note also the presence of the volume V in the above definitions. In the one-phase region ($\eta_p^r < \eta_{p,cr}^r$), the distribution $P(\eta_c)$ will lose its bimodal structure and become single peaked. In this regime the correct definition for the susceptibility reads [3, 4]:

$$\chi_c = V \left[\left(\int_0^{\infty} \eta_c^2 P(\eta_c) d\eta_c \right) - \langle \eta_c \rangle^2 \right], \quad (13)$$

with $\langle \eta_c \rangle$ given by Eq.(3).

The above definitions are easily modified to define the corresponding observables for the polymer phases (simply replace the subscript “c” by “p”). Since our simulations also store the polymer histograms, coexisting packing fractions and susceptibilities can be calculated for these phases as well. Note that the above definitions are additionally attractive from a numerical point of view because the integrations over η_c tend to average out the statistical fluctuations that may be present in $P(\eta_c)$.

The interfacial tension is extracted from the logarithm of the probability distribution: $W \equiv \ln P(\eta_c)$. Since W corresponds to the free energy of the system, the height of the peaks in W may be identified as the free energy barrier separating the colloidal vapor from the colloidal liquid [27]. In Fig. 1 the barrier is marked F_L , where the subscript L emphasizes that the data stem from a finite simulation box of size L . In practice, F_L is extracted from W via:

$$F_L = W_+ - W_-, \quad (14)$$

where W_+ is the average of W in the peaks: $W_+ = (W_v + W_l)/2$, and W_- the value of W at the minimum between the peaks (the symbols W_v and W_l are defined in Fig. 1). The corresponding interfacial tension for the finite system reads [27]:

$$\sigma_L = F_L / (2L^2), \quad (15)$$

where the factor of two stems from the use of periodic boundary conditions which yield the formation of two interfaces in the system.

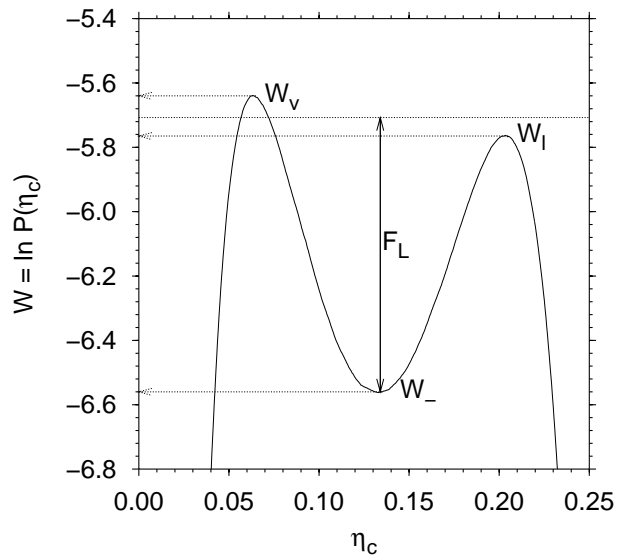


FIG. 1: Logarithm of the probability distribution $W \equiv \ln P(\eta_c)$ for an AO model with $q = 0.8$ and $\eta_p^r = 0.765$ at coexistence. The data were obtained in a cubic simulation cell with edge $L = 21.0$ and using periodic boundary conditions. The peak at low η_c corresponds to the colloidal vapor, the peak at high η_c to the colloidal liquid. W_v (W_l) denotes the maximum value of the colloidal vapor (liquid) peak. W_- is the minimum value of W between the two peaks. F_L corresponds to the free energy barrier separating the vapor phase from the liquid phase.

V. CRITICAL BEHAVIOR

Essential in the study of critical phenomena is some measure of distance from the critical point. As measure of distance we use in this work the parameter:

$$t = (\eta_p^r / \eta_{p,cr}^r - 1), \quad (16)$$

which is positive in the two-phase region ($\eta_p^r > \eta_{p,cr}^r$) and negative in the one-phase region ($\eta_p^r < \eta_{p,cr}^r$). This implies that in the one-phase region we must use $-t$.

When the critical point is approached from the two-phase region, M and σ vanish precisely, while χ diverges. Common symbols have been established to denote the critical exponents and critical amplitudes of the associated power laws:

$$M = Bt^\beta, \quad \sigma = \sigma_0 t^{2\nu}, \quad \chi = (\Gamma^-) t^{-\gamma}, \quad (17)$$

where hyperscaling has been assumed (valid for systems that belong to the 3D Ising universality class).

When the critical point is approached from the other side, namely the one-phase region, M and σ remain zero, while χ diverges:

$$\chi = \Gamma^+ (-t)^{-\gamma}, \quad (18)$$

but with a different critical amplitude Γ^+ .

The critical behavior of the coexistence diameter D in the two-phase region is given by [28, 29]:

$$D - X_{\text{cr}} = At^{1-\alpha}, \quad (19)$$

with X_{cr} the packing fraction at criticality, given by $\eta_{c,\text{cr}}$ ($\eta_{p,\text{cr}}$) in case of the colloid (polymer) coexistence diameter. In the one-phase region D is not well defined because the distinction between a colloidal vapor and liquid is then no longer possible.

For the 3D Ising universality class, the critical exponents are given by:

$$\begin{aligned} \beta &= 0.324, & \gamma &= 1.239, \\ \nu &= 0.629, & \alpha &= 0.113. \end{aligned} \quad (20)$$

Also certain combinations of the critical amplitudes are universal [11, 12, 13]. Of importance in this work are the ratios:

$$U_2 = \Gamma^+/\Gamma^- \approx 4.76 \pm 0.24, \quad (21)$$

$$w^2 R_\sigma^{3/2} = \frac{\sigma_0^{3/2} \Gamma^-}{B^2} \approx 0.13 \pm 0.04, \quad (22)$$

$$\frac{(R_\sigma^+)^{3/2}}{Q_c} = \frac{\sigma_0^{3/2} \Gamma^+}{B^2} \approx 0.71 \pm 0.13, \quad (23)$$

with values taken from Ref. 11, where $k_B T$ is used as the unit of energy. The ranges represent the spread in different estimates obtained from experiment, simulation, and theory. Note that the ranges are quite substantial, indicating that the determination of critical amplitudes is still a challenge.

VI. FINITE SIZE SCALING

In a computer simulation, the critical power laws given in the previous section cannot be observed directly. As explained before, this is related to the correlation length which diverges at the critical point and hence cannot be captured in a finite system of size L . However, it is possible to perform several simulations at different system sizes and use the predictions of finite size scaling theory to extrapolate to the thermodynamic limit. Reviews of the subject are abundant in the literature [3, 4, 5]. In this section, we will therefore be brief and only reproduce the equations required for our analysis.

A. Finite size scaling of M , χ and D

According to finite size scaling theory, the order parameter M_L obtained in a finite system of linear dimension L close to the critical point shows a systematic L dependence that can be written as [5]:

$$M_L = L^{-\beta/\nu} \mathcal{M}^0(tL^{1/\nu}), \quad (24)$$

with t the distance from the critical point, critical exponents $\{\beta, \nu\}$ and \mathcal{M}^0 some function independent of system size (\mathcal{M}^0 is called a scaling function). The critical exponents appropriate for the AO model are the 3D Ising exponents listed in Eq.(20). Since \mathcal{M}^0 is system size-independent, this implies that plots of $L^{\beta/\nu} M_L$ versus $tL^{1/\nu}$ should all collapse onto one master curve, provided the correct values of the critical polymer fugacity and the critical exponents are used. Such scaling plots [4] thus give an indication of whether the assumed universality class is indeed correct. Moreover, for large $tL^{1/\nu}$ (but still within the critical region of course) such plots should approach the power law behavior of the thermodynamic limit. This is best visualized if a double logarithmic scale in the scaling plot is used. The data should then approach a straight line, with slope β and intercept equal to the critical amplitude B .

The scaling behavior of the susceptibility is analogously given by:

$$\chi_L = L^{\gamma/\nu} \chi^0(tL^{1/\nu}). \quad (25)$$

In this case, the appropriate quantities for the scaling plot are $L^{-\gamma/\nu} \chi_L$ and $tL^{1/\nu}$. On a double logarithmic scale, the data should approach a straight line, with slope $-\gamma$ and intercept equal to the critical amplitude Γ^- or Γ^+ (depending on whether the critical point is approached from the one-phase or the two-phase region).

By presenting the simulation data in the form of scaling plots, measurements of the critical amplitudes become possible. The accuracy of the method increases when larger system sizes are used. In order for finite size scaling theory to apply, it is important that the simulations are performed in the so-called scaling regime. At which system size L the scaling regime begins, varies from system to system and is *a priori* not known. If, however, the considered system sizes are too small, it will show in the corresponding scaling plots as systematic deviations from any data collapse onto a master curve. Alternatively, one could consider corrections to finite size scaling theory for these smaller systems [30].

In principle, a finite size scaling analysis of the coexistence diameter D is also possible. In this case, the appropriate scaling plot is $(D - X_{\text{cr}})L^{(1-\alpha)/\nu}$ expressed as a function of $tL^{1/\nu}$. In practice, however, it is difficult to distinguish in simulation data the term $t^{1-\alpha}$ in Eq.(19) from the next order term in the series expansion (which would be linear in t) because the critical exponent α is rather small. The accuracy of such scaling plots is therefore usually rather poor.

B. Finite size scaling of σ

The interfacial tension in the thermodynamic limit σ_∞ (in d dimensions) is related to the free energy barrier of the finite system F_L via [27]:

$$\exp(F_L) = AL^x \exp(2L^{d-1} \sigma_\infty), \quad (26)$$

where trivial factors of $k_B T$ have been dropped. Taking the logarithm on both sides, the above equation can be written as:

$$\sigma_L = \sigma_\infty + \frac{x \ln L}{2L^{d-1}} + \frac{\ln A}{2L^{d-1}}, \quad (27)$$

with σ_L the interfacial tension of the finite system given by Eq.(15) and constants $\{x, A\}$ that are generally not known. While it is not possible to measure σ_∞ directly, it is possible to measure the interfacial tension of the finite system σ_L for several system sizes L , and then use the above equation to extrapolate to the thermodynamic limit.

One attractive feature of Eq.(27) is that it does not depend on the critical exponent ν and can therefore be applied without prior knowledge of the universality class of the system. In other words, it can be used to measure ν as is demonstrated in Ref. 31 for the Lennard-Jones fluid. For the AO model, the universality class is already known [8, 9]. In this case, Eq.(27) still provides a powerful consistency check: if the universality class of the AO model is indeed 3D Ising, it should be possible to extract the exponent ν from the simulation data.

The issue here is how to perform the extrapolations in practice [32, 33, 34]. Ideally, the simulation data for the different system sizes should be extrapolated to the thermodynamic limit using two-parameter fits in the variables $\ln(L)/L^{d-1}$ and $1/L^{d-1}$. This approach, however, may have numerical problems associated with it. Typically, only data over a relatively small range of different system sizes is available (this is certainly the case for a non-trivial mixture like the AO model). It will be difficult to separate the $\ln(L)/L^{d-1}$ term accurately from the $1/L^{d-1}$ term over such a small range. Therefore, this extrapolation scheme will likely lead to poor precision.

Alternatively, one can argue that for small L it may occur that $|x \ln L| < |\ln A|$, in which case an extrapolation in the single variable $1/L^{d-1}$ is most appropriate, whereas for large L the single variable $\ln(L)/L^{d-1}$ is the better choice [27]. In Ref. 31, for example, the extrapolations are performed in the single variable $\ln(L)/L^{d-1}$. Since it is *a priori* not clear which of the above extrapolation methods is the most accurate, all are investigated in this work.

VII. RESULTS

The following results stem from simulations of the AO model with $q = 0.8$ performed in cubic boxes with edge length L and using periodic boundary conditions. The dimensionality of the simulations is $d = 3$. In order to apply finite size scaling, the following system sizes are considered: $L_1 = 15.5$, $L_2 = 16.7$, $L_3 = 17.7$ and $L_4 = 21.0$. For each system size, the coexistence probability $P(\eta_c)$ is measured accurately at one value of η_p^r chosen in the vicinity of the critical point. Histogram reweighting is used to extrapolate $P(\eta_c)$ to other values of η_p^r . We also

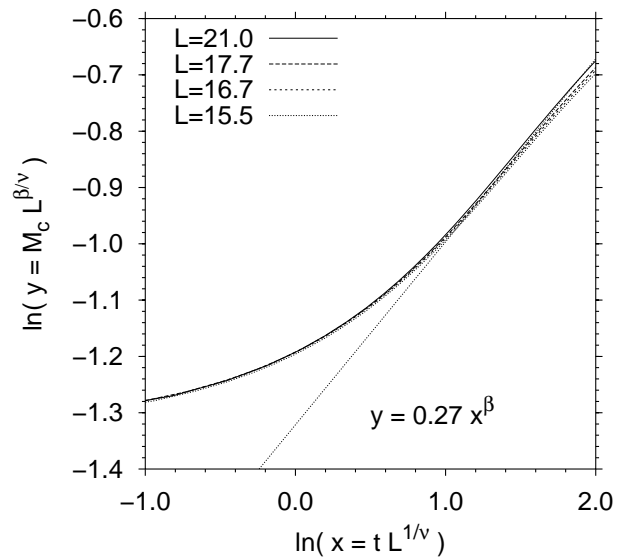


FIG. 2: 3D Ising scaling plot for the order parameter of the colloids M_c given by Eq.(9) for the AO model with $q = 0.8$ in the two-phase region. The choice of axis is explained in the text. The critical amplitude is extracted by means of a fit to the tail of the data, see also Table I.

performed a number of shorter simulations to explicitly measure $P(\eta_c)$ at different values of η_p^r . The results of these simulations were used to check the consistency and accuracy of the extrapolated distributions. The quality of our data is such that extrapolations over the range $\eta_p^r \approx 0.72$ to $\eta_p^r \approx 0.83$ can be carried out reliably.

A. Order parameter and binodal

The critical behavior of the order parameter of the colloids M_c is analyzed in the scaling plot of Fig. 2. The collapse of the simulation data from the different system sizes onto one master curve is clearly visible. The scaling plot for the order parameter of the polymers M_p is shown in Fig. 3, which again demonstrates the collapse onto one master curve. In these figures, the critical polymer fugacity $\eta_{p,cr}^r$ was used as a free parameter and tuned until the best collapse occurred. By performing a linear least squares fit to the tails of the master curves, the critical amplitudes can be obtained. The corresponding critical power laws are given in Table I, which also lists the value of $\eta_{p,cr}^r$ that was used in the scaling plots. Naturally, this value of $\eta_{p,cr}^r$ should agree with the previous estimate listed in Eq.(2). The critical amplitudes obtained from the fits are sensitive to the range over which the fit is performed: the variation is used as a measure for the error in Table I.

The critical behavior of the coexistence diameter of the colloids D_c is presented in Fig. 4. In this case, the best collapse of the data occurs at $\eta_{p,cr}^r = 0.771$ which

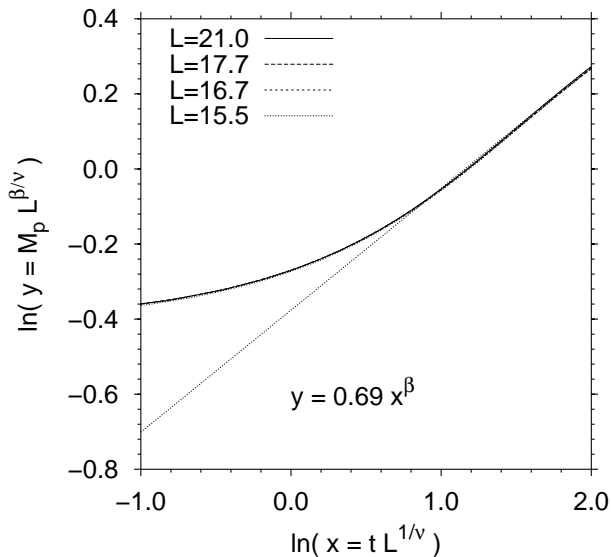


FIG. 3: The analogue of Fig. 2 for the order parameter of the polymers M_p .

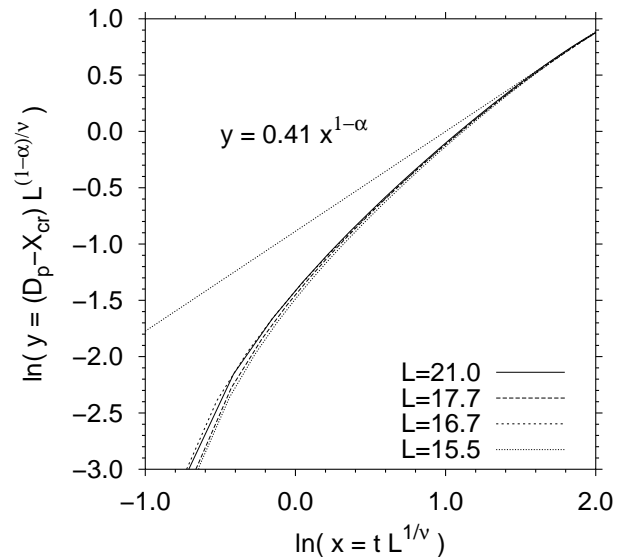


FIG. 5: The analogue of Fig. 4 for the coexistence diameter of the polymers D_p . $X_{cr} = \eta_{p,cr}$ was taken from Eq.(2).

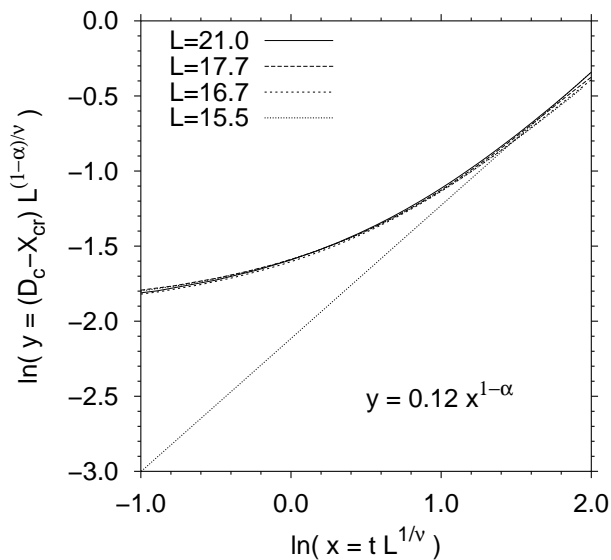


FIG. 4: Scaling plot of the coexistence diameter of the colloids D_c . The value of $X_{cr} = \eta_{c,cr}$ used in this plot was taken from Eq.(2). Allowing variations in X_{cr} did not improve the collapse of the data.

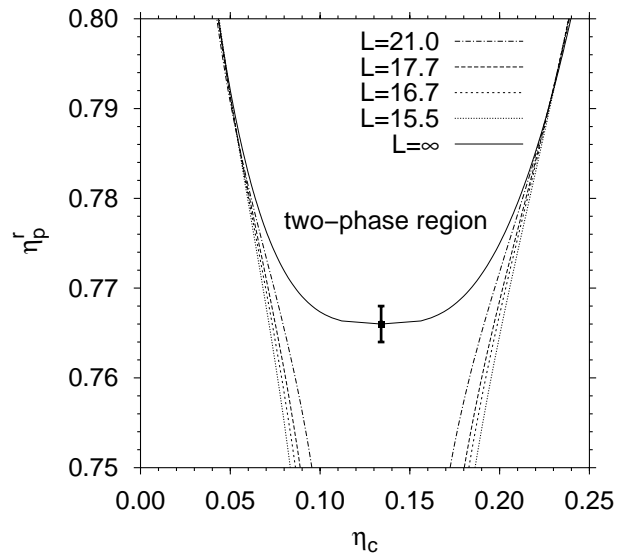


FIG. 6: Phase diagram of the AO model in reservoir representation. The solid curve ($L = \infty$) shows the binodal in the thermodynamic limit obtained using the power laws for M_c and D_c listed in Table I (here $\eta_{p,cr}^r = 0.766$ was used). The dashed/open curves are raw simulation data for various finite system sizes L as indicated. The bar marks the location of the critical point given by Eq.(2).

is not in agreement with Eq.(2). Some discrepancy is to be expected though because the singularity in the coexistence diameter is very weak, which makes it hard to discern it from simulation data. The behavior of the data in the tails, however, seems rather well described by the exponent $1 - \alpha$. The corresponding scaling plot for the coexistence diameter of the polymers D_p is shown in Fig. 5. In this case, the curvature of the data for small t seems in error. Therefore, we conclude that our simula-

tion data is not accurate enough to reliably extract the critical behavior of the coexistence diameter. The power laws for D_c and D_p , given for completeness in Table I, must therefore be treated with some care.

By combining the expressions for M_c and D_c in Table I, the colloid packing fractions of the vapor and liq-

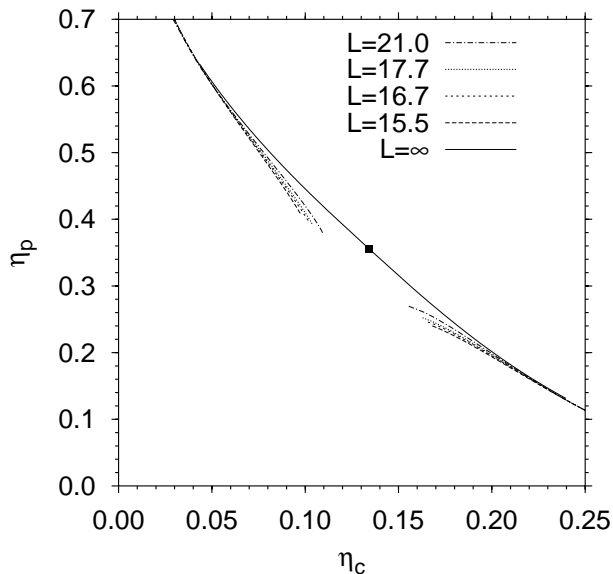


FIG. 7: Phase diagram of the AO model in system representation. The solid curve ($L = \infty$) shows the binodal in the thermodynamic limit obtained using finite size scaling (here $\eta_{p,cr}^r = 0.766$ was used). The dashed/open curves are raw simulation data for various finite system sizes L as indicated. The square marks the location of the critical point given by Eq.(2).

uid phase (η_c^v and η_c^l) can be written as functions of η_p^r . These expressions, which are valid close to the critical point in the thermodynamic limit, describe the binodal of the AO model in reservoir representation. The resulting binodal is shown in Fig. 6, together with the raw simulation data from the various system sizes. The figure clearly shows the familiar finite-size deviation of the simulation data close to the critical point [4]. If also the critical expressions for M_p and D_p are used, η_p^r can be eliminated altogether to yield the binodal in the experimentally more relevant (η_c, η_p) or system representation. The resulting plot is shown in Fig. 7, together with the raw simulation data.

B. Susceptibility

Next, we consider the critical behavior of the susceptibility. Fig. 8 shows the scaling plot of the susceptibility of the colloidal phase χ_c in the one-phase region. The critical power law extracted from this plot is listed in Table I. The scaling plot for the susceptibility of the polymer phase χ_p in the one-phase region is qualitatively similar and not shown. Instead, only the critical power law is given in Table I.

Measurements of the susceptibility in the two-phase region are prone to a number of potential numerical pitfalls. Since the susceptibility is a second order moment of the distribution $P(\eta_c)$, it is generally more sensitive to

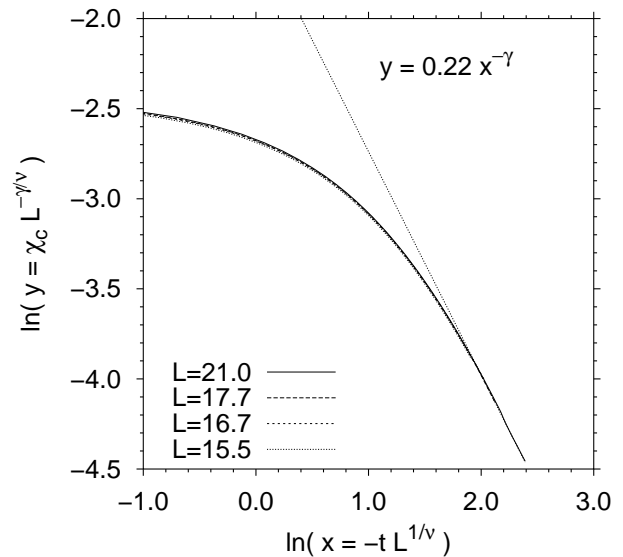


FIG. 8: Scaling plot of the susceptibility of the colloidal phase χ_c in the one-phase region. In this case Eq.(13) is used to measure χ_c .

statistical errors than first order moments like the order parameter. For asymmetric systems like the AO model, the additional problem arises that the statistics in the liquid peak of $P(\eta_c)$ are systematically better than in the vapor peak: simply because the liquid peak contains more colloids. These problems will of course vanish with increasing system size. However, for a non-trivial system like the AO model, the system sizes that can be handled today are unfortunately still in the regime where these subtleties come into play.

In case of the colloidal vapor and liquid in the two-phase region, the relevant susceptibilities are χ_c^v given by Eq.(11) and χ_c^l given by Eq.(12). In principle, close to the critical point, the susceptibility should be the same in both phases. In practice, there will be differences due to the numerical difficulties outlined above. Two procedures are now conceivable: (1) use the average of χ_c^v and χ_c^l as best estimate of the susceptibility, or (2) use only χ_c^l . Which of these procedures is the best needs to be checked with the data available. In our case, the susceptibility of the colloidal phase in the two-phase region was best described using only χ_c^l . The resulting scaling plot is shown in Fig. 9 and the corresponding power law in Table I. The collapse of the data is clearly visible, but unlike Fig. 8, the slope of the data for large t is not quite $-\gamma$. A less satisfactory fit is expected though, because the statistics in Fig. 9 are significantly worse compared to Fig. 8 since only half the data is used.

The susceptibility measurements of the polymer phases in the two-phase region were most accurate if the average $\chi_p^{\text{II}} \equiv (\chi_p^l + \chi_p^v)/2$ was used. The scaling plot of χ_p^{II} is shown in Fig. 10 and the corresponding power law is listed in Table I. As in Fig. 9, the data collapse is clearly

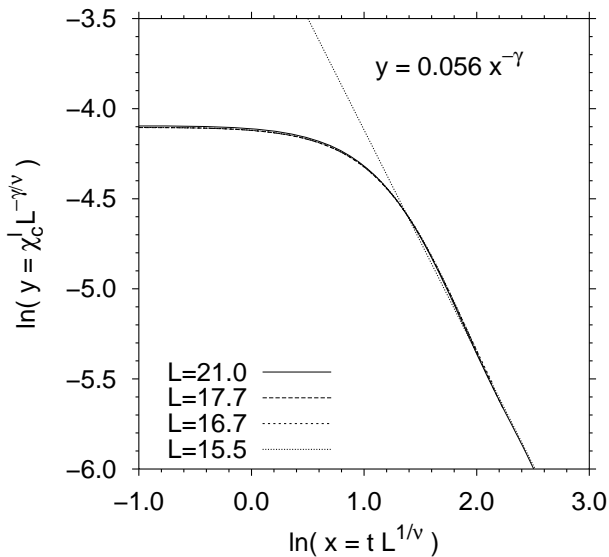


FIG. 9: Scaling plot of the susceptibility of the colloidal liquid χ_c^I given by Eq.(12) in the two-phase region.

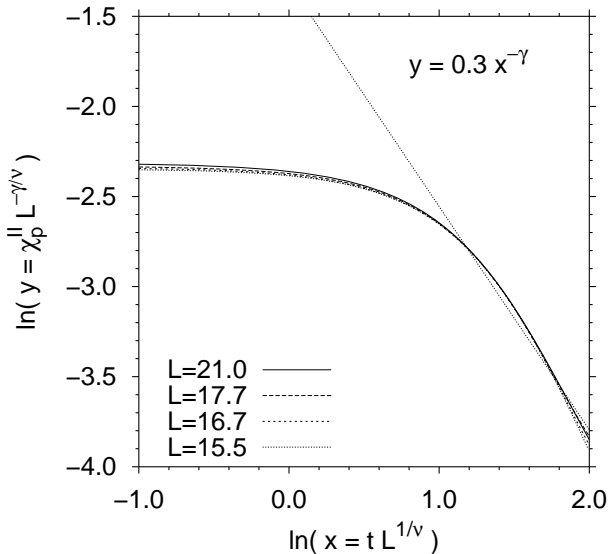


FIG. 10: Scaling plot of the average susceptibility of the two polymer phases χ_p^{II} in the two phase region.

demonstrated, but the slope $-\gamma$ is not quite reproduced.

In Fig. 11 we plot the susceptibility of the colloids as function of η_p^r in the vicinity of the critical point. Shown are the raw simulation data as well as the critical power laws of Table I. Clearly demonstrated is the familiar finite-size rounding of the raw simulation data in the vicinity of the singularity [4].

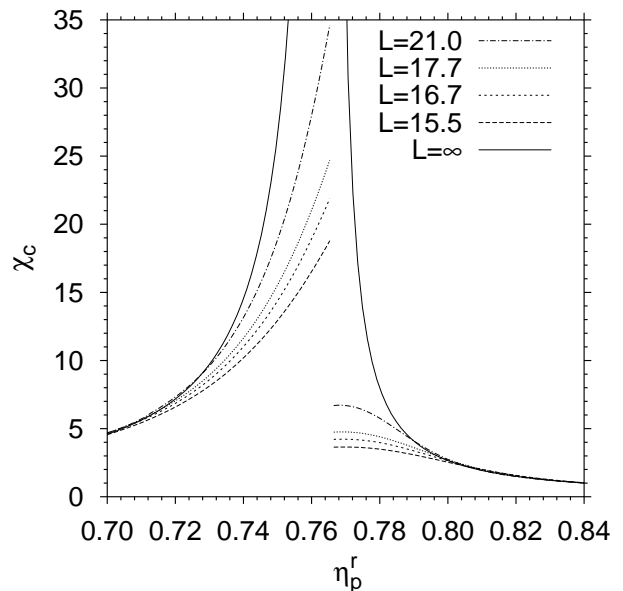


FIG. 11: Susceptibility of the colloids χ_c across the phase transition. The solid curve shows the susceptibility in the thermodynamic limit given by the critical power laws of Table I with $\eta_{p,cr}^r = 0.766$. The remaining curves show the raw simulation data of the various system sizes L .

C. Interfacial tension

As mentioned before, the finite size extrapolation of the interfacial tension is less straightforward and various methods can be used. Since the number of different system sizes considered by us is rather small, multi-parameter fits such as the ones investigated in Ref. 33 are out of the question. Instead, we investigate single parameter fits only, which in this case essentially means choosing $\ln(L)/L^{d-1}$ or $1/L^{d-1}$ as scaling variable. The results of both extrapolation procedures for a number of different η_p^r are summarized in Fig. 12 and Fig. 13. The extrapolations produce meaningful estimates up to $\eta_p^r \approx 0.80$. For higher values of η_p^r , one leaves the critical regime and Eq.(27) breaks down. In this regime, the interfacial tension gradually becomes system size independent.

The fits in Fig. 12 and Fig. 13 seem equally accurate, and based on these figures alone we cannot reject one extrapolation method in favor of the other. The issue is resolved when the interfacial tension σ_∞ in the thermodynamic limit itself is considered. In this case, the critical power law $\sigma_\infty = \sigma_0 t^{2\nu}$ is valid which implies that plots of σ_∞ versus t on double logarithmic scales should collapse onto straight lines, provided the correct value of $\eta_{p,cr}^r$ in t is used. Note that $\eta_{p,cr}^r$ is the only free parameter: the critical exponent ν follows automatically from the slope of the line. The resulting plots are shown in Fig. 14 and Fig. 15, in which $\ln(L)/L^{d-1}$ and $1/L^{d-1}$ were used as scaling variable, respectively, and $\eta_{p,cr}^r$ in each plot was

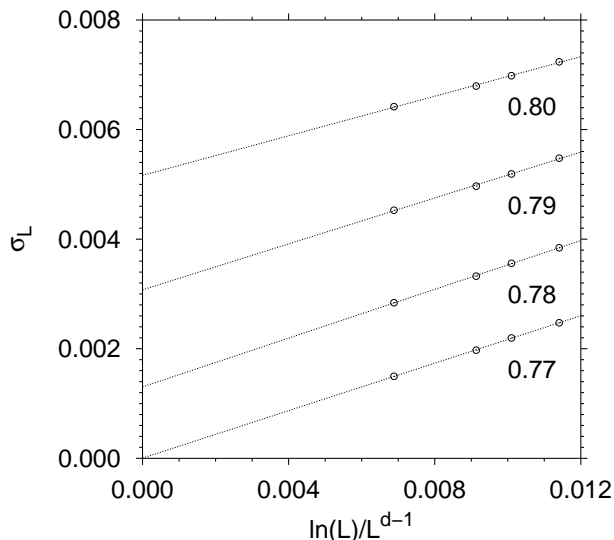


FIG. 12: Finite size extrapolation of the interfacial tension in $\ln(L)/L^{d-1}$. This extrapolation scheme corresponds to the assumption $\ln A = 0$ in Eq.(27). Shown in the above plot is the interfacial tension of the finite system σ_L as function of $\ln(L)/L^{d-1}$ for various values of η_p^r as indicated. The straight lines are linear least squares fits to the data. The intercept of these lines with the ordinate yields an estimate for the interfacial tension σ_∞ in the thermodynamic limit.

tuned until the best collapse occurred. In these figures, measurements of the interfacial tension up to $\eta_p^r = 0.79$ were used.

One important observation is that both data sets in Fig. 14 and Fig. 15 accurately reproduce the expected slope $2\nu \approx 1.26$ corresponding to 3D Ising behavior. However, if $\ln(L)/L^{d-1}$ is used as scaling variable, the best collapse is obtained at $\eta_{p,\text{cr}}^r = 0.7696$, which is not in agreement with the previous estimate of Eq.(2). On the other hand, if $1/L^{d-1}$ is used, the best collapse is observed at $\eta_{p,\text{cr}}^r = 0.7661$, which is in excellent agreement with Eq.(2). Therefore, we conclude that $1/L^{d-1}$ is the appropriate scaling variable for our problem. The corresponding power law obtained from Fig. 15 is listed in Table I. The effect of using the incorrect scaling variable seems to be that the critical point is not correctly estimated, while the critical exponent is less affected. It thus seems wise practice to always compare the critical point obtained from finite size extrapolations of the interfacial tension to some other independent estimate (this estimate could for instance be obtained using the cumulant intersection method).

It is worth noting that Berg *et al.* in Ref. 33 also conclude that the extrapolation of the interfacial tension is most consistent if $x = 0$ is assumed in Eq.(27). In retrospect, it is not surprising that $1/L^{d-1}$ is the appropriate scaling variable in our case. Close to the critical point, the distribution $P(\eta_c)$ scales with the system size

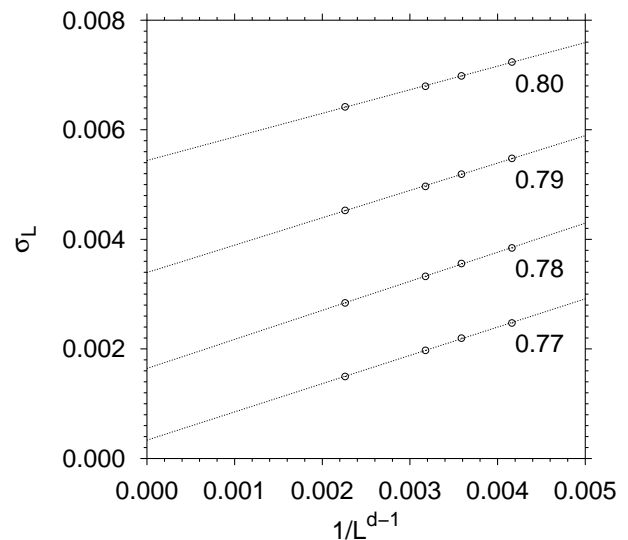


FIG. 13: The analogue of Fig. 12 but using $1/L^{d-1}$ as scaling variable instead. This extrapolation scheme corresponds to the assumption $x = 0$ in Eq.(27).

as [21, 35, 36]:

$$P_L(\eta_c) = b_0 L^{\beta/\nu} \mathcal{P}^0(b_0 L^{\beta/\nu} \eta_c), \quad (28)$$

where $P_L(\eta_c)$ is the distribution $P(\eta_c)$ measured in the finite system of size L , b_0 some non-universal constant, and \mathcal{P}^0 a function independent of system size. According to Eq.(14), the free energy barrier F_L is given by the peak-to-valley height in the logarithm of $P_L(\eta_c)$. The above scaling property thus implies that F_L becomes L independent close to the critical point. As a result, the

TABLE I: Summary of the critical behavior of the AO model with $q = 0.8$. Shown are the critical power laws in the one-phase and two-phase regions of various physical quantities obtained in scaling plots. Listed in the last column is the value of $\eta_{p,\text{cr}}^r$ at which the best collapse in the corresponding scaling plot was observed (provided here to give an indication of the consistency of our results). The symbols M , D , χ and σ are defined in section IV, while the critical exponents are listed in Eq.(20).

| | one-phase region | two-phase region | $\eta_{p,\text{cr}}^r$ |
|----------------------------|---------------------------------|--------------------------------|------------------------|
| M_c | – | $(0.27 \pm 0.02)t^\beta$ | 0.765 |
| M_p | – | $(0.69 \pm 0.01)t^\beta$ | 0.765 |
| $D_c - \eta_{c,\text{cr}}$ | – | $(0.12 \pm 0.01)t^{1-\alpha}$ | 0.771 |
| $D_p - \eta_{p,\text{cr}}$ | – | $(0.41 \pm 0.01)t^{1-\alpha}$ | 0.766 |
| χ_c | $(0.22 \pm 0.03)(-t)^{-\gamma}$ | $(0.056 \pm 0.005)t^{-\gamma}$ | 0.766 |
| χ_p | $(1.24 \pm 0.08)(-t)^{-\gamma}$ | $(0.3 \pm 0.1)t^{-\gamma}$ | 0.765 0.768 |
| σ | – | $(0.26 \pm 0.02)t^{2\nu}$ | 0.766 |

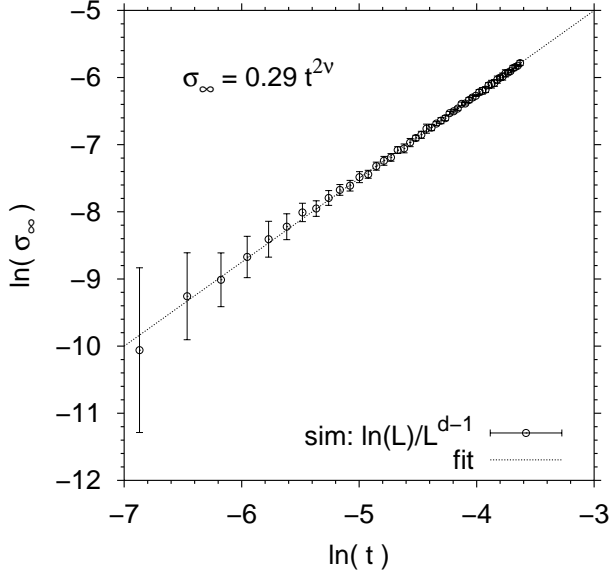


FIG. 14: Interfacial tension in the thermodynamic limit σ_∞ as function of t on a double logarithmic scale, where $\ln(L)/L^{d-1}$ was used as scaling variable. The best collapse onto a straight line is observed at $\eta_{p,cr}^r = 0.7696$, which is not in agreement with Eq.(2). The slope of the line yields the critical exponent of the interfacial tension, for which we find $2\nu = 1.25 \pm 0.01$.

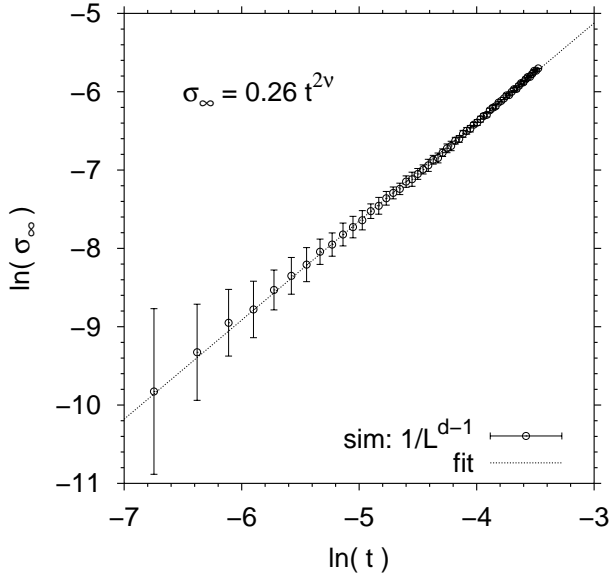


FIG. 15: The analogue of Fig. 14 in which $1/L^{d-1}$ is used as scaling variable instead. The best collapse occurs at $\eta_{p,cr}^r = 0.7661$, which is in excellent agreement with Eq.(2). For the critical exponent we obtain $2\nu = 1.26 \pm 0.01$ and for the critical amplitude $\sigma_0 = 0.26 \pm 0.02$.

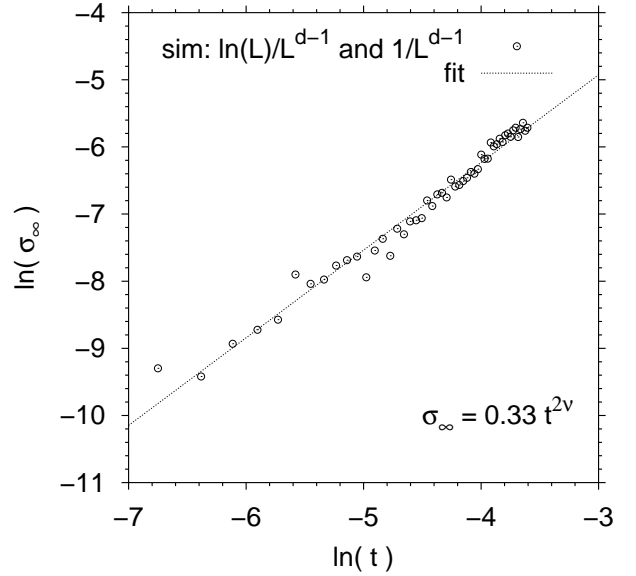


FIG. 16: The analogue of Fig. 14 using two parameter fits in $\ln(L)/L^{d-1}$ and $1/L^{d-1}$ when extrapolating the interfacial tension to the thermodynamic limit. The best collapse occurs at $\eta_{p,cr}^r = 0.7689$. For the critical exponent we obtain $2\nu = 1.30 \pm 0.04$ and for the critical amplitude $\sigma_0 = 0.33 \pm 0.03$.

interfacial tension should scale with $1/L^{d-1}$.

For completeness, we also show in Fig. 16 the behavior of σ_∞ as function of t when two-parameter fits in both $\ln(L)/L^{d-1}$ and $1/L^{d-1}$ are used. Since only four different system sizes are considered, the statistical quality of the extrapolations will likely deteriorate, and this clearly shows in Fig. 16. Still, even then, it is possible to extract the critical exponent and the critical point with reasonable accuracy. Note that the deviations in $\eta_{p,cr}^r$ obtained using the various extrapolation schemes are below the one percent level. In practice, the choice of extrapolation scheme thus only becomes important when high resolution data are available.

D. Critical amplitude ratios

We now turn to the critical amplitude ratios that can be extracted from Table I. We first calculate U_2 given by Eq.(21). If we consider the colloidal phases we obtain $U_2 = 3.9 \pm 0.9$. The corresponding ratio for the polymers is found to be $U_2 = 4.1 \pm 1.9$. Within the error bars, these estimates are compatible with Eq.(21). The quantity $w^2 R_\sigma^{3/2}$ is found to be 0.10 ± 0.04 for the colloidal phases, and 0.08 ± 0.04 for the polymer phases. This is again compatible with Eq.(22), although one must be aware of the large error bars in our estimates. Finally, the quantity $(R_\sigma^+)^{3/2}/Q_c$ is found to be 0.40 ± 0.16 for the colloids, and 0.35 ± 0.07 for the polymers. In this case, we systematically underestimate the values listed

in Eq.(23). Note, however, that the discrepancy with the 3D Ising values is not too severe. Given the difficulty in general of measuring critical amplitudes, even in the case of simple lattice models [11], the agreement we obtain is already quite remarkable.

VIII. SUMMARY AND OUTLOOK

In summary, we have studied the critical behavior of the order parameter, interfacial tension, susceptibility and coexistence diameter of the AO model with colloid to polymer size ratio $q = 0.8$. An important result is that the critical exponent of the interfacial tension equals the expected 3D Ising value $2\nu \approx 1.26$. This critical behavior is consistent with previous simulations [8, 9], and also with experimental work [37] in which 3D Ising critical behavior was observed in real colloid-polymer mixtures. The critical behavior of the order parameter and the susceptibility are also 3D Ising like. Our data for the coexistence diameter is not conclusive. This is related to the small value of the critical exponent α , which makes it difficult to accurately resolve the critical behavior from the simulation data. More accurate simulations of larger systems are required to resolve this.

We found that the critical amplitude ratios obtained from our simulations are compatible with the 3D Ising universality class. This confirms the consistency of our data, and is encouraging considering the AO model is an asymmetric binary mixture and therefore difficult to simulate. We emphasize, however, that our estimates for the critical amplitudes should be regarded as consistency checks only. Their accuracy cannot compete with that obtained in, for example, direct simulations of the 3D

Ising lattice model.

We have demonstrated that finite size scaling methods are equally applicable to rather complex systems like the AO model, and can be used to obtain results with meaningful accuracy. Regarding finite size extrapolations of the interfacial tension, our analysis is consistent with Ref. 33, in the sense that the most consistent fits are obtained by ignoring the $\ln(L)$ dependent term in Eq.(27). For the AO model, we also observed that by using the incorrect scaling variable, the critical point in particular is not estimated correctly.

This work provides additional insight into the critical behavior of the AO model. For a complete understanding, the critical behavior of the correlation length should still be investigated. While the corresponding critical exponent is of course known, namely $-\nu$, the critical amplitude is not. This critical amplitude, however, cannot be extracted from the probability distribution $P(\eta_c)$. The usual approach to study the correlation length is to consider the static structure factor instead [26]. This requires additional simulations which are beyond the scope of this work, and will be postponed to a future publication.

Acknowledgments

We are grateful to the Deutsche Forschungsgemeinschaft for support (TR6/A5) and to M. Müller for many stimulating discussions. Generous allocation of computer time on the JUMP cluster at the Forschungszentrum Jülich GmbH is gracefully acknowledged. We also thank K. Dawson, R. Evans, and M. Schmidt for stimulating remarks.

-
- [1] A. P. Gast, C. K. Hall, and W. B. Russel, *J. Colloid Interface Sci.* **96**, 215 (1983).
- [2] W. C. K. Poon, *Current Opinion in Colloid & Interface Science* **3**, 593 (1998).
- [3] K. Binder and E. Luijten, *Phys. Rep.* **344**, 179 (2001).
- [4] H-P. Deutsch, *J. Stat. Phys.* **67**, 1039 (1992).
- [5] D. P. Landau and K. Binder, *A Guide to Monte Carlo Simulations in Statistical Physics* (Cambridge University Press, Cambridge, 2000).
- [6] S. Asakura and F. Oosawa, *J. Chem. Phys.* **22**, 1255 (1954).
- [7] A. Vrij, *Pure Appl. Chem.* **48**, 471 (1976).
- [8] R. L. C. Vink and J. Horbach, *J. Phys.: Condens. Matter*, in press (2004).
- [9] R. L. C. Vink and J. Horbach, *J. Chem. Phys.* **121**, 3253 (2004).
- [10] J. M. Brader, R. Evans, and M. Schmidt, *Mol. Phys.* **101**, 3349 (2003).
- [11] A. Pelissetto and E. Vicari, *Phys. Rep.* **368**, 549 (2002).
- [12] D. Stauffer, M. Ferer, and M. Wortis, *Phys. Rev. Lett.* **29**, 345 (1972).
- [13] V. Privman, P. C. Hohenberg, and A. Aharony, in *Phase Transitions and Critical Phenomena*, Eds. C. Domb and J. L. Lebowitz (Academic Press, London, 1991).
- [14] P. Virnau and M. Müller, *J. Chem. Phys.* **120**, 10925 (2004).
- [15] M. Müller and N. B. Wilding, *Phys. Rev. E* **51**, 2079 (1995).
- [16] H. Lekkerkerker, W. Poon, P. Pusey, A. Stroobants, and P. Warren, *Europhys. Lett.* **20**, 559 (1992).
- [17] E. Meijer and D. Frenkel, *J. Chem. Phys.* **100**, 6873 (1994).
- [18] M. Schmidt, H. Löwen, J. Brader, and R. Evans, *Phys. Rev. Lett.* **85**, 1934 (2000).
- [19] P. Bolhuis, A. Louis, and J-P. Hansen, *Phys. Rev. Lett.* **89**, 128302 (2002).
- [20] M. Schmidt, A. Fortini, and M. Dijkstra, *J. Phys.: Condens. Matter* **15**, S3411 (2003).
- [21] K. Binder, *Z. Phys.* **B43**, 119 (1981).
- [22] N. Wilding, *Ann. Rev. Comp. Phys.* **IV**, p. 37 (1996).
- [23] R. E. Goldstein and N. W. Ashcroft, *Phys. Rev. Lett.* **55**, 2164 (1985).
- [24] R. L. C. Vink, in *Computer Simulation Studies in Condensed Matter Physics XVIII*, Eds. D.P. Landau, S.P.

- Lewis, and H.B. Schuettler (Springer Verlag, Heidelberg, Berlin, 2004).
- [25] A. M. Ferrenberg and R. H. Swendsen, *Phys. Rev. Lett.* **61**, 2635 (1988).
- [26] S. K. Das, J. Horbach, and K. Binder, *J. Chem. Phys.* **119**, 1547 (2003).
- [27] K. Binder, *Phys. Rev. A* **25**, 1699 (1982).
- [28] M. Nakata, T. Dobashi, N. Kuwahara, M. Kaneko, and B. Chu, *Phys. Rev. A* **18**, 2683 (1978).
- [29] J. J. Rehr and N. D. Mermin, *Phys. Rev. A* **8**, 472 (1973).
- [30] E. Luijten, M. Fisher, and A. Panagiotopoulos, *Phys. Rev. Lett.* **88**, 185701 (2002).
- [31] J. Potoff and A. Panagiotopoulos, *J. Chem. Phys.* **112**, 6411 (2000).
- [32] K. K. Mon, *Phys. Rev. Lett.* **60**, 2749 (1988).
- [33] B. A. Berg, U. Hansmann, and T. Neuhaus, *Phys. Rev. B*, **47**, 497 (1993).
- [34] J. E. Hunter III and W. P. Reinhardt, *J. Chem. Phys.* **103**, 8627 (1995).
- [35] D. Nicolaides and A. D. Bruce, *J. Phys. A* **21**, 233 (1988).
- [36] A. D. Bruce and N. B. Wilding, *Phys. Rev. Lett.* **68**, 193 (1992).
- [37] B.H. Chen, B. Payandeh, and M. Robert, *Phys. Rev. E* **62**, 2369 (2000).